days.) It is not known exactly why these measurements should be polarity dependent; however, the correct explanation probably has to do with the built-in asymmetry in the waveguide/electrode structure. One possible explanation is that the ITO/NLO interface is acting primarily as a hole injector.[46] If this is true, space charge buildup in the NLO film would be more pronounced with the ITO electrode positive than with the ITO electrode negative. This would result in a smaller average electric field inside the NLO film and a lower apparent electrooptic coefficient for ITO positive. An alternative explanation is that a larger space charge built up in the monomer glass because hole mobility is much larger than electron mobility in this layer.[47] A larger space charge in the monomer glass buffer would force a larger field across the NLO film and would result in a larger apparent electrooptic coefficient. Indeed, any combination of these two effects (i.e., hole injection into the NLO or into the monomer glass buffer) could explain the observed polarity dependence.

Conclusions

We have successfully synthesized polymers bearing pendant chromophores with strong NLO activity. The moderately large electrooptic coefficients measured for poled samples of these polymers could be predicted with reasonable accuracy based on measurements of molecular properties (μ_g and β) and linear optical properties of the materials. However, because of assumptions and uncertainties inherent to the calculations, discrepancies between predicted and experimental values of r_{33} cannot be attributed solely to nonelectronic contributions. Prototype electrooptic devices have been constructed, but it is clear that stronger chromophores and improved stability of alignment will be required for any practical applications. Studies directed to address these issues and to investigate the dynamics of the orientation of these polymers are in progress and will be reported later.

Acknowledgment. We express our appreciation to M. Thomas and J. Reiff for SEC measurements, to V. Mazzio and M. Moscato for DSC measurements, and to S. B. Crayton and E. J. Voll for density measurements, all members of Eastman Kodak Analytical Technology Division. We acknowledge J. O'Reilly for DSC measurements on polymer 1, and E. Prince for preparing the ITO layers used in waveguiding experiments, both of Eastman Kodak Corporate Research Laboratories. We also thank C. A. Maggulli, M. Lodollini, and D. White of the GLM Telesis Co. for synthetic assistance.

Registry No. 1 (homopolymer), 139278-65-2; 2 (homopolymer), 139278-66-3; 3 (copolymer), 139278-67-4; 4 (copolymer), 139278-68-5; 5 (copolymer), 139278-69-6; 6, 122-98-5; 7, 93-90-3; 8, 120654-22-0; 9, 5470-49-5; 10, 139278-57-2; 11, 139278-55-0; 12, 139278-56-1; 13, 139278-59-4; 14, 139278-60-7; 15, 139278-58-3; 16, 139278-61-8; acryloyl chloride, 814-68-6.

(46) Tang, C. W.; VanSlyke, S. A. *Appl. Phys. Lett.* **1987**, *51*, 913.
(47) Stolka, M.; Yanus, J. F.; Pai, D. M. *J. Phys. Chem.* **1984**, *88*, 4707.

Structure and Properties of the Transition-Metal Zintl Compounds: $A_{14}MnBi_{11}$ (A = Ca, Sr, Ba)

Traci Y. Kuromoto,[†] Susan M. Kauzlarich,*[,†] and David J. Webb*[,‡]

Departments of Chemistry and Physics, University of California, Davis, California 95616

Received October 10, 1991. Revised Manuscript Received December 9, 1991

$A_{14}MnBi_{11}$ (A = Ca, Sr, Ba) is synthesized by reacting the elements in stoichiometric amounts at high temperatures (950–1350 °C). Single-crystal X-ray diffraction data (130 K, a = 17.002 (6) Å, c = 22.422 (7) Å (Ca); a = 17.820 (6) Å, c = 23.394 (6) Å (Sr); a = 18.633 (8) Å, c = 24.340 (10) Å (Ba)) were refined (tetragonal, $I4_1/acd(142)$, Z = 8, R = 5.4%, R_w = 5.9% (Ca), R = 4.1%, R_w = 4.7% (Sr), R = 5.1%, R_w = 4.9% (Ba)) and showed these compounds to be isostructural to the main-group analogues, $Ca_{14}AlSb_{11}$ and $A_{14}GaAs_{11}$ (A = Ca, Sr). Magnetization measurements performed on powder samples have shown that $Ca_{14}MnBi_{11}$ and $Sr_{14}MnBi_{11}$ are ferromagnets and that $Ba_{14}MnBi_{11}$ is an antiferromagnet. The magnetic coupling between Mn ions is attributed to an RKKY interaction, and thus metallic behavior is expected. The temperature dependence of the resistivity of pressed pellets is presented and suggests that all three compounds are metals.

Introduction

Many bonding schemes have been suggested for the wide variety of materials that exist. These vary from the Hume-Rothery[1] rules for intermetallic compounds to the simple valence rules for insulating compounds.[2] There are a large number of solid-state compounds whose structures can be understood by a simple electron-counting scheme referred to as the Zintl concept.[3,4] The initial suggestions of E. Zintl concerned binary compounds composed of an alkali or alkaline earth metal and a main-group element. Zintl proposed that the structures and properties of these phases could be understood by considering the compound to be composed of an electropositive metal which transfers its electrons to the electronegative element which in turn forms the correct number of homoatomic bonds such that each element has a complete octet.[5] The

[†] Department of Chemistry.
[‡] Department of Physics.
* To whom correspondence should be addressed.

(1) Hume-Rothery, W. *J. Inst. Met.* **1926**, *35*, 313.
(2) Pauling, L. *The Nature of the Chemical Bond*, 3rd ed.; Cornell University Press: Cornell University, 1960.
(3) (a) Schäfer, H.; Eisenmann; B.; Müller, W. *Angew. Chem., Int. Engl.* **1973**, *12*, 694, (b) Schäfer, H.; Eisenmann, B. *Rev. Inorg. Chem.* **1981**, *3*, 29, (c) Schäfer, H. *Annu. Rev. Mater, Sci.* **1985**, *15*, 1, (d) Schäfer, H. *J. Solid State Chem.* **1985**, *57*, 97.
(4) Nesper, R. *Prog. Solid State Chem.* **1990**, *20*, 1.
(5) Zintl, E. *Angew. Chem.* **1939**, *52*, 1.

0897-4756/92/2804-0435$03.00/0

Zintl concept has been expanded to include more complicated ternary materials and is sometimes referred to as the Zintl–Klemm[4,6] or the Zintl–Klemm–Bussmann[3a,7] concept, henceforth collectively referred to as the Zintl concept. Generally, Zintl phases can be separated from either the insulators or the typical intermetallic phases because they are described by simple valence rules and are expected to be semiconductors, although relatively few compounds have been extensively characterized.[3,4] The ability to dissolve Zintl compounds into coordinating solvents such as ethylenediamine[8] is another property which sets these compounds apart from intermetallics. These solvated Zintl anions are useful starting materials in the synthesis of new compounds[8,9] and the metallization of polymer substrates.[10]

The Zintl concept has been extended to include transition-metal compounds with some success.[11] In an effort to test the limits of the Zintl concept as it applies to transition-metal compounds, we have prepared a series of ternary manganese bismuth compounds which are isostructural to the main-group Zintl compounds, $Ca_{14}AlSb_{11}$[12] and $A_{14}GaAs_{11}$ (A = Ca, Sr).[13] There are relatively few ternary transition-metal bismuth compounds. In the solid state, a series of ternary manganese bismuth compounds, $A^{II}MnBi_2$ (A^{II} = Ca, Sr), $CaMn_2Bi_2$, and $Ca_9Mn_4Bi_9$ have been reported[14] as well as some ternary alkali-metal bismuth compounds, $A^{I}MnBi$ (A^{I} = alkali metal),[15] Li_2AgBi, and Li_2AuBi.[16] However, the structures of these compounds cannot be understood by using the Zintl concept. Preliminary accounts of the structure and some properties of $Ca_{14}MnBi_{11}$ have been reported.[17] $Ca_{14}MnBi_{11}$ is metallic and ferromagnetic with $T_c \approx 55$ K and is the first example of a transition-metal compound that is isostructural to a main-group Zintl compound. The relatively strong magnetic coupling must be due to the fact that the compound is a metal because the closest Mn···Mn distance is about 10 Å, but metallic behavior is surprising considering that the structure can be described within the Zintl concept. To determine the origin of the magnetic and electronic properties of this compound, we have synthesized two new compounds, $Sr_{14}MnBi_{11}$ and $Ba_{14}MnBi_{11}$. In this paper we compare the structure and properties of $Sr_{14}MnBi_{11}$ and $Ba_{14}MnBi_{11}$ with $Ca_{14}MnBi_{11}$.

Experimental Section

Materials. The elements Ca (99.99%), Sr (99.95%), Ba (99.9%), and Bi (99.999%) were obtained from Anderson Physics Labs. Manganese pieces (99.98%) from Johnson Matthey were first cleaned in a 5% HNO_3/MeOH solution and immediately transferred into the drybox.

Synthesis. Bismuth needles and the cleaned manganese flakes were ground into powders and the alkaline-earth elements were cut into small pieces in a nitrogen-filled drybox. $Ca_{14}MnBi_{11}$, $Sr_{14}MnBi_{11}$, and $Ba_{14}MnBi_{11}$ were prepared by enclosing stoichiometric amounts of the elements in welded niobium tubes which were first cleaned with an acid solution (20% HF, 25% HNO_3, and 55% H_2SO_4). The niobium tube was then sealed in a quartz ampule under a vacuum or low pressures ($\sim^1/_5$ atm) of Ar. High yields (>95%) of X-ray-quality black needle or polygonal single crystals were obtained by slowly heating (1 °C/min) the mixtures to 1350 °C with a dwelling time of 2 h. The reaction was then quickly cooled to room temperature. Crystals of $Ca_{14}MnBi_{11}$ were black polygons; the crystals of $Sr_{14}MnBi_{11}$ were black needles, and the crystals of $Ba_{14}MnBi_{11}$ were highly reflective, bronze-colored polygons and needles. Lower temperatures (950 °C) for longer dwell times (4–7 days) provided high yields (>95%) of polycrystalline pieces. The reactants and products were handled in a nitrogen-filled drybox when not sealed in the niobium containers.

X-ray Diffraction. X-ray powder diffraction patterns (room temperature, monochromatic Cu $K\alpha_1$ radiation, λ = 1.540 56 Å) were obtained with an Enraf-Nonius Guinier powder camera. The sample was mounted between two pieces of tape with silicon included as an internal standard. The powder patterns were indexed according to information obtained from the single-crystal structural refinements. The positions and intensities of the experimental diffraction lines agreed very well with the calculated diffraction pattern based on the single-crystal X-ray structure.[18] The corresponding room-temperature lattice constants were determined by standard least-squares refinement[19] and are given in Table I.

The air-sensitive crystals were coated with oil in the drybox to protect them from air. A suitable crystal was mounted on a glass fiber with silicone grease and positioned in a cold stream of nitrogen. The single-crystal diffraction data for $Ca_{14}MnBi_{11}$ were collected at 130 K on a Syntex $P2_1$ diffractometer (Mo $K\alpha$, λ = 0.710 69 Å, graphite monochromator). The crystal lattice was determined to be orthorhombic F by the automatic indexing

Table I. Some Crystal and Refinement Data for $A_{14}MnBi_{11}$ (A = Ca, Sr, Ba)

	$Ca_{14}MnBi_{11}$[a]	$Sr_{14}MnBi_{11}$	$Ba_{14}MnBi_{11}$
space group, Z	$I4_1/acd$, 8	$I4_1/acd$, 8	$I4_1/acd$, 8
T, K	130	130	130
a, Å[b]	17.002 (6)	17.820 (6)	18.633 (8)
c, Å[b]	22.422 (7)	23.394 (8)	24.340 (10)
V, Å^3	6481 (4)	7427 (4)	8450 (6)
μ(Mo Kα), cm^{-1}	590	718	586
transm coeff range	0.23–0.43	0.13–0.47	0.20–0.36
$2\theta_{max}$	50	55	55
no. obsd refns	758 ($I > 2.5\sigma I$)	1042 ($I > 3\sigma I$)	1810 ($I > 3\sigma I$)
no. params refined	61	61	61
R,[c] %	5.4	4.1	5.1
R_w,[c] % [$w = 1/s^2(F_o)$]	5.9	4.7	4.9

[a] The data were collected in the orthorhombic crystal lattice (a = 24.054 (8), b = 24.034 (8), and c = 22.420 (7) Å) and subsequently transformed to the tetragonal crystal lattice outlined in Table I. [b] Room-temperature lattice dimensions were obtained from Guinier powder diffraction. $Ca_{14}MnBi_{11}$: a = 17.066 (2) Å, c = 22.498 (4) Å. $Sr_{14}MnBi_{11}$: a = 17.847 (1) Å, c = 23.442 (3) Å. $Ba_{14}MnBi_{11}$: a = 18.665 (3) Å, c = 24.429 (Å). [c] $R = \sum||F_o| - |F_c||/|F_c|$ and $R_w = \sum||F_o| - |F_c||w^{1/2}/\sum|F_o w^{1/2}|$.

(6) Klemm, W. *Proc. Chem. Soc. London* **1958**, 329.
(7) Busmann, E. *Z. Anorg. Allg. Chem.* **1961**, *313*, 90.
(8) Corbett, J. D. *Chem. Rev.* **1985**, *85*, 383.
(9) (a) Whitmire, K. H.; Churchill, M. R.; Fettinger, J. C. *J. Am. Chem. Soc.* **1985**, *107*, 1056. (b) Flomer, W. A.; O'Neall, S. C.; Kolis, J. W.; Jeter, D.; Cordes, A. W. *Inorg. Chem.* **1988**, *27*, 969. (c) Eichhorn, B. W.; Haushalter, R. C.; Cotton, F. A.; Wilson, B. *Inorg. Chem.* **1988**, *27*, 4084. (d) Flomer, W. A.; Kolis, J. W. *J. Am. Chem. Soc.* **1988**, *110*, 3682. (e) Eichhorn, B. W.; Haushalter, R. C.; Pennington, W. T. *J. Am. Chem. Soc.* **1988**, *110*, 8704.
(10) Haushalter, R. C.; Krause, L. J. *Thin Solid Films* **1983**, *102*, 161.
(11) Brönger, W. *Pure Appl. Chem.* **1985**, *57*, 1363.
(12) Cordier, G.; Schäfer, H.; Stelter, M. *Z. Anorg. Allg. Chem.* **1984**, *519*, 183.
(13) (a) Kauzlarich, S. M.; Thomas, M. M.; Odink, D. A.; Olmstead, M. M. *J. Am. Chem. Soc.* **1991**, *113*, 7205. (b) Kauzlarich, S. M.; Kuromoto, T. Y. *Croat. Chim. Acta.*, in press.
(14) (a) Brechtel, E., Cordier, G.; Schäfer, H. *Z. Naturforsch.* **1980**, *35b*, 1. (b) Cordier, G.; Schäfer, H. *Z. Naturforsch.* **1976**, *31b*, 1459. (c) Brechtel, E.; Cordier, G.; Schäfer, H. *Z. Naturforsch.* **1979**, *34b*, 1229.
(15) Achenbach, Von G.; Schuster, H.-U. *Z. Anorg. Allg. Chem.* **1981**, *475*, 9.
(16) Pauly, H.; Weiss, A.; Witte, H. *Z. Metallkd.* **1968**, *59*, 47.
(17) (a) Kauzlarich, S. M.; Kuromoto, T. Y.; Olmstead, M. M. *J. Am. Chem. Soc.* **1989**, *111*, 8041. (b) Kuromoto, T. Y.; Kauzlarich, S. M.; Webb, D. J. *Mol. Cryst. Liq. Cryst.* **1990**, *181*, 349. (c) Webb, D. J.; Kuromoto, T. Y.; Kauzlarich, S. M. *J. Magn. Magn. Mater.* **1991**, *98*, 71.
(18) Clark, C. M.; Smith, D. K.; Johnson, G. J. *A FORTRAN II Program for calculating X-ray diffraction Patterns, Version 5*; Department of Geosciences: Pennsylvania State University, University Park, PA, 1973.
(19) Cell parameters were obtained by indexing the powder patterns with the least-squares program LATT. Takusagawa, F.; Corbett, J. D. Iowa State University, 1981, unpublished.

Table II. Atomic Coordinates (×10⁴) and Isotropic Equivalent Thermal Parameters (Å² × 10³)

atom	x	y	z	U[a]
		$Ca_{14}MnBi_{11}$		
Bi(1)	1388 (1)	−6114 (1)	1250	11 (1)
Bi(2)	62 (1)	1083 (1)	8103 (1)	11 (1)
Bi(3)	8701 (1)	9725 (1)	9531 (1)	11 (1)
Bi(4)	0	2500	1250	10 (1)
Mn	5000	2500	1250	12 (2)
Ca(1)	1759 (5)	2906 (4)	5778 (4)	13 (2)
Ca(2)	9776 (5)	1235 (4)	37 (4)	15 (2)
Ca(3)	3536 (6)	0	2500	11 (3)
Ca(4)	8221 (4)	899 (5)	8429 (3)	13 (2)
		$Sr_{14}MnBi_{11}$		
Bi(1)	1360 (1)	−6142 (1)	1250	10 (1)
Bi(2)	51 (1)	1106 (1)	8121 (1)	11 (1)
Bi(3)	8691 (1)	9732 (1)	9530 (1)	13 (1)
Bi(4)	0	2500	1250	11 (1)
Mn	5000	2500	1250	15 (3)
Sr(1)	1766 (2)	2917 (2)	5781 (1)	10 (1)
Sr(2)	9770 (1)	1237 (2)	19 (1)	11 (1)
Sr(3)	3534 (2)	0	2500	9 (2)
Sr(4)	8211 (2)	923 (2)	8429 (1)	11 (2)
		$Ba_{14}MnBi_{11}$		
Bi(1)	1329 (1)	−6174 (1)	1250	3 (1)
Bi(2)	35 (1)	1137 (1)	8146 (1)	4 (1)
Bi(3)	8676 (1)	9739 (1)	9534 (1)	3 (1)
Bi(4)	0	2500	1250	6 (1)
Mn	5000	2500	1250	2 (3)
Ba(1)	1775 (1)	2930 (1)	5780 (1)	3 (1)
Ba(2)	9790 (1)	1244 (2)	−9 (1)	6 (1)
Ba(3)	3569 (1)	0	2500	3 (1)
Ba(4)	8198 (1)	916 (1)	8436 (1)	5 (1)

[a] Equivalent isotropic U defined as one-third of the trace of the orthogonalized U_{ij} tensor.

routine of the diffractometer software. Unit cell parameters were obtained from least-squares refinement of about 15 reflections with 20° <2θ < 35°. Initially, the structure of $Ca_{14}MnBi_{11}$ was solved by direct methods which provided the Bi positions. Fourier maps provided the lighter atoms in the orthorhombic space group *Fddd* (a = 24.054 (8) Å, b = 24.034 (8) Å, and c = 22.420 (7) Å, Z = 16). It was recognized that the structure was analogous to $Ca_{14}AlSb_{11}$, and the data were subsequently transformed to the tetragonal space group $I4_1/acd$ (a = 17.002 (6) Å and c = 22.422 (7) Å, Z = 8). Single-crystal diffraction data on $Sr_{14}MnBi_{11}$ and $Ba_{14}MnBi_{11}$ were collected at 130 K on a Siemens R3m/v diffractometer (Mo Kα, λ = 0.710 69 Å, graphite monochromator) equipped with a modified LT-1 low-temperature apparatus. The unit cell parameters of the Sr and Ba analogues were obtained from least-squares refinement of about 15–20 reflections with 20° <2θ < 35°. The I centering was verified in all cases from axial photographs and systematic extinctions. No decomposition of the crystal for any of the compositions was observed (inferred from the intensity of two check reflections). Crystallographic parameters are summarized in Table I. The data were corrected for Lorentz and polarization effects. Crystallographic programs used were those of SHELXTL Version 5.0 installed on a Data General eclipse or Micro VAX computer. Scattering factors and corrections for anomalous dispersion were from ref 20.

The initial atomic positions for the Sr and Ba analogues were taken from $Ca_{14}MnBi_{11}$ and refined by least-squares methods. An absorption correction[21] was applied after the refinement converged with isotropic U's and all atoms were then refined with anisotropic U's. The largest feature in the final difference map for the Ca and Sr analogues is 4 e/Å³ and is located between 1 and 2 Å from the central bismuth in the linear chain. The final difference map for $Ba_{14}MnBi_{11}$ contained large peaks (10 e/Å³) which are located 2 Å from either a barium or bismuth atom. These large peaks are attributed to problems due to absorption, and since the structure is confirmed by the room-temperature powder diffraction data, a second single-crystal data set was not obtained. Atomic coordinates and isotropic thermal parameters are given in Table II. The anisotropic thermal parameters and the observed and calculated structure factor amplitudes for each structural solution are available as supplementary material (see paragraph at end of paper).

Magnetic and Electrical Characterization. Magnetization measurements were made on a Quantum Design SQUID magnetometer at temperatures of 5–300 K. The samples were sealed in fused silica tubes under vacuum. Magnetization versus magnetic field measurements were obtained at 6 K in order to estimate the saturation magnetization.

Electrical resistivity measurements were made on pellets of $Sr_{14}MnBi_{11}$ and $Ba_{14}MnBi_{11}$ cold-pressed to 10 000 psi and on a polycrystalline piece of $Ca_{14}MnBi_{11}$. A four-probe in-line method was used for measuring the samples. A current of 5 mA (Keithley Model 224 current source) was applied, and the voltage was measured with a Keithley Model 181 nanovoltmeter for 10 K ≤ T ≤ 300 K. Samples were mounted in the drybox onto a sample holder which could be sealed in the drybox to protect them from air and moisture. Indium was placed on the tips of four spring steel leads which were clamped down onto the sample. The sealed sample holder was then transferred to the closed cycle refrigerator. The sample was first cooled to 10 K and then the resistivity was measured every 1 °C near the magnetic ordering temperatures and every 5 °C up to 300 K. All samples exhibited ohmic behavior.

Results and Discussion

$Ca_{14}MnBi_{11}$ was initially synthesized in low yield by reacting the elements Ca, Mn, and Bi in the molar ratio of 9:4:9 (Ca:Mn:Bi). Crystals suitable for single-crystal X-ray diffraction were obtained, and the structure was determined by a combination of direct methods for the heavy atoms and subsequent Fourier maps. Once the structure and composition were determined, high yields (>95% as determined by Guinier powder diffraction) of $Ca_{14}MnBi_{11}$ could be obtained by reacting the stoichiometric combination of the elements. Measurement of the magnetic and electronic properties indicated ferromagnetic and metallic behavior[17] and were the impetus for attempting the synthesis of the series of compounds $A_{14}MnBi_{11}$ (A = Sr, Ba). The synthesis of the A = Mg compound has not been attempted. High yields (>95% as determined by Guinier powder diffraction) of $Sr_{14}MnBi_{11}$ and $Ba_{14}MnBi_{11}$ could be obtained by reacting the stoichiometric combination of the elements. Small amounts of the oxide, A_4Bi_2O,[22] were identified as an impurity in some of the reactions, but rigorous cleaning and drying procedures eliminates this impurity. The $Ba_{14}MnBi_{11}$ compound appears to be more air sensitive than either $Sr_{14}MnBi_{11}$ or $Ca_{14}MnBi_{11}$ and would "tarnish" over 24 h in a nitrogen drybox (Vacuum Atmosphere, typical H_2O content <1 ppm).

Structural Results. The compounds, $A_{14}MnBi_{11}$ (A = Ca, Sr, or Ba) can be described according to the Zintl concept as consisting of 14 A^{2+}, 4 Bi^{3-}, $MnBi_4^{9-}$, and Bi_3^{7-}. The structure can be described as consisting of alkaline earth atoms, isolated Bi atoms, distorted $MnBi_4$ tetrahedra, and Bi_3 linear chains. Selected bond distances and angles can be found in Table III. Figure 1 shows a perspective along the c axis of the packing of atoms and polyatomic anions in the unit cell: the $MnBi_4$ tetrahedra are translated by $^1/_2$ along the c axis alternating with the Bi_3 anions which are rotated by 90° with respect to each other. The isolated

(20) *International Tables for X-ray Crystallography*; Kynoch Press: Birmingham, England, 1974; Vol. IV.

(21) The absorption correction is made using Program XABS: Hope, H.; Moezzi, B. The program obtains an absorption tensor from $F_o - F_c$ differences: Moezzi, B. Ph.D. Dissertation University of California, Davis, CA, 1987.

(22) Ca_2Bi has been reported but assumed to be Ca_4Bi_2O, analogous to Ca_4Sb_2O: (a) Eisenmann, B.; Schäfer, H. *Z. Naturforsch.* **1974**, *29b*, 13. (b) Eisenmann, B.; Limartha, H.; Schäfer, H. *Z. Natuforsch.* **1980**, *35b*, 1518.

Table III. Selected Bond Distances (Å) and Angles (deg)

	$Ca_{14}MnBi_{11}$	$Sr_{14}MnBi_{11}$	$Ba_{14}MnBi_{11}$
Bi(1)-Bi(4)	3.335 (2)	3.425 (2)	3.498 (1)
Bi(1)-A(1) (×2)	3.288 (8)	3.428 (3)	3.567 (1)
Bi(1)-A(2) (×2)	3.370 (8)	3.518 (3)	3.707 (2)
Bi(1)-A(3) (×2)	3.384 (1)	3.565 (1)	3.751 (1)
Bi(1)-A(4) (×2)	3.221 (7)	3.407 (3)	3.601 (2)
Bi(2)-A(1)	3.228 (8)	3.404 (3)	3.590 (1)
Bi(2)-A(1′)	3.250 (8)	3.447 (3)	3.659 (2)
Bi(2)-A(2)	3.865 (8)	4.012 (3)	4.097 (2)
Bi(2)-A(2′)	3.218 (8)	3.347 (3)	3.492 (2)
Bi(2)-A(3)	3.301 (7)	3.502 (3)	3.705 (2)
Bi(2)-A(4)	3.229 (7)	3.373 (3)	3.518 (2)
Bi(2)-A(4′)	3.453 (8)	3.582 (3)	3.740 (2)
Bi(3)-A(1)	3.291 (8)	3.429 (3)	3.585 (2)
Bi(3)-A(1′)	3.265 (8)	3.414 (3)	3.558 (2)
Bi(3)-A(2)	3.349 (8)	3.492 (3)	3.660 (2)
Bi(3)-A(2′)	3.211 (8)	3.408 (3)	3.585 (2)
Bi(3)-A(3)	3.201 (7)	3.342 (3)	3.496 (2)
Bi(3)-A(4)	3.279 (8)	3.445 (3)	3.573 (2)
Bi(3)-A(4′)	3.267 (7)	3.400 (3)	3.540 (2)
Bi(3)-A(4″)	3.794 (8)	3.995 (3)	4.145 (2)
Bi(4)-A(1) (×4)	3.247 (8)	3.415 (3)	3.590 (1)
Bi(4)-A(2) (×4)	3.489 (8)	3.679 (3)	3.877 (1)
Mn-Bi(2) (×4)	2.814 (1)	2.889 (1)	2.935 (1)
Mn-A(2)	3.618 (8)	3.747 (3)	3.841 (1)
Mn···Mn	10.183 (3)	10.658 (3)	11.128 (3)
Bi(2)-Mn-Bi(2′)	118.0 (1)	118.7 (1)	119.9 (1)
Bi(2)-Mn-Bi(2″)	105.4 (1)	105.0 (1)	104.5 (1)

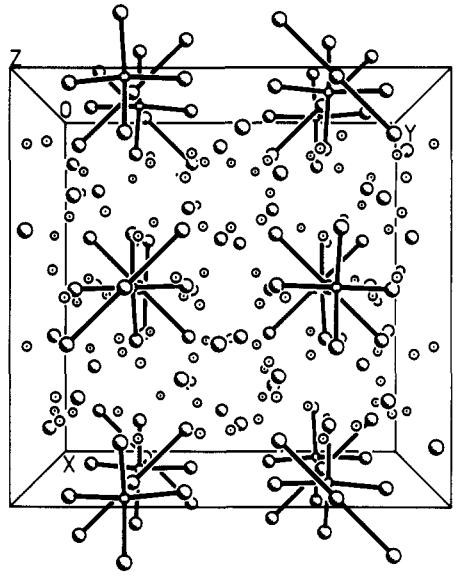

Figure 1. Perspective view of the unit cell down the *c* axis of $Sr_{14}MnBi_{11}$. The shaded, open, and dotted circles represent Bi, Mn, and Sr atoms, respectively.

Bi atoms can also be seen in Figure 1 and are situated between the Bi_3 units and the $MnBi_4$ tetrahedra. In the unit cell, these Bi atoms are located along a screw axis and form a spiral coincident with the *c* axis.

Figure 2 shows a perspective view down the *b* axis (top) and a [001] projection down the *c* axis (bottom) of the polyatomic anions and associated atoms for a formula unit. There are some general trends in bond distances and angles across the series of compounds. The $MnBi_4^{9-}$ tetrahedra are slightly distorted and are flattened along the *a*–*b* plane. As the cation size increases, this distortion increases by about 1°. There are four cations (A(2) in Table III) located close to the Bi(2) atoms in the tetrahedron. They are close to and slightly above and below the flattened tetrahedron. The tetrahedra in $Ca_{14}AlSb_{11}$[12] and $A_{14}GaAs_{11}$ (A = Ca, Sr)[13] are also slightly distorted. The main-group Bi analogues have not been reported.

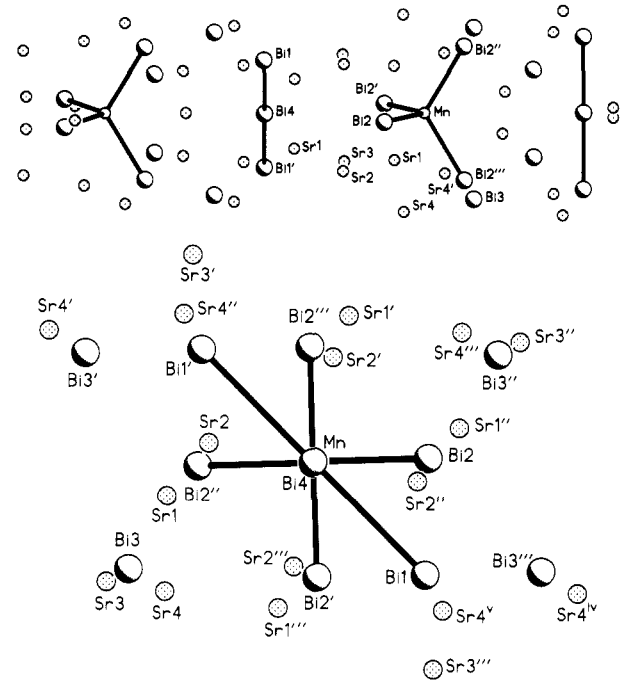

Figure 2. Top: perspective view down the *b* axis of polyatomic anions with surrounding Bi^{3-} and Sr^{2+} ions. Bottom: [001] projection of the polyatomic anions with surrounding Bi^{3-} and Sr^{2+} ions.

Although the distortion of the tetrahedron has been attributed to a Jahn–Teller effect for a d^4 ion ($Mn^{III}Bi_4$)[9-17a] it may also be due to steric effects. In addition, as the cation size and electron donating ability increases, the Mn–Bi bond distance lengthens by about 0.1 Å (2.814 (1) Å (Ca), 2.889 (1) Å (Sr), and 2.935 (1) Å (Ba)). Typical Mn–Bi bond lengths range from 2.82 to 2.96 Å in Ca–Mn–Bi compounds.[14] The Zintl concept describes the role of the cations in these structures exclusively as electron donors to the more electronegative units. Therefore, as the cation is changed from a weaker electron donor, Ca, to a stronger electron donor, Ba, the cation is able to donate more electron density to the Bi atoms of the tetrahedron which results in greater electron repulsion between the Mn and Bi atoms, and a lengthening of the Mn–Bi distances. The increasing bond length as a function of increasing cation size and decreasing electronegativity is also observed in $A_{14}CaAs_{11}$ (A = Ca, Sr)[13b] as well as in other cation series in Zintl compounds.[3,7,23]

The Bi–Bi distances in the linear chains also increase from 3.335 (2) Å (A = Ca) to 3.425 (2) Å (A = Sr), to 3.498 (1) Å (A = Ba) as a function of increasing cation size and electron donor ability for the same reasons as described above. The Bi–Bi distances in the linear chain for $Ca_{14}MnBi_{11}$ are comparable with bonding interactions observed in $Ca_{11}Bi_{10}$,[24] which range from 3.15 to 3.34 Å and, for $Sr_{14}MnBi_{11}$ and $Ba_{14}MnBi_{11}$, with the second coordination of Bi found in Bi metal (3.53 Å).[25] These long Bi–Bi bonds for the Bi_3^{7-} anion are consistent with the interpretation of either a three-center four-electron hypervalent bond[26] or dsp^3 hybridization about the central Bi. Although several examples of pnictogen compounds have been shown

(23) Witte, J.; von Schnering, H. V. *Z. Anorg. Allg. Chem.* **1964**, *327*, 260.
(24) Deller, K.; Eisenmann, B. *Z. Naturforsch.* **1976**, *31B*, 29.
(25) Curka, P.; Barrett, C. S. *Acta Crystallogr.* **1962**, *15*, 865.
(26) (a) Pimentel, G. C. *J. Chem. Phys.* **1951**, *19*, 446. (b) Rundle, R. E. *Surv. Prog. Chem.* **1963**, *1*, 81. (c) Gabes, W.; Nijman-Meester *Inorg. Chem.* **1973**, *12*, 589. (d) Cahill, P. A.; Dykstra, C. E.; Martin, J. C. *J. Am. Chem. Soc.* **1985**, *107*, 6359.

Table IV. Magnetic Parameters and Room-Temperature Resistivity Values

	$Ca_{14}MnBi_{11}$	$Sr_{14}MnBi_{11}$	$Ba_{14}MnBi_{11}$
μ_{eff},[a] (μ_B)	4.8 (1)	5.0 (1)	4.8 (1)
T_C or T_N, K	55	33	15
θ, K	50 (1)	38 (1)	17 (1)
μ_s, μ_B	2.50	2.70	2.9
χ_0,[b] emu/mol	0.005 (2)	0.0057 (1)	0.0035 (5)
ρ_{300K}, Ω cm	8 (2) × 10^{-4}	1 (1) × 10^{-2}	1 (1) × 10^{-2}

[a] Using the equation $\mu_{eff} = (8C)^{1/2}$. [b] Obtained from fitting the data to the equation $\chi = \chi_0 + C/(T - \theta)$.

to possess this dsp^3 hybridization,[27] theoretical calculations on $Ca_{14}GaAs_{11}$[28] indicate that it is more appropriate to view the bonding within the X_3^{7-} group as a three-center four-electron hypervalent bond. The large formal charge on this Bi_3^{7-} anion is apparently stabilized by several A–Bi(4) (central Bi) and A–Bi(1) (terminal Bi) interactions. The central Bi(4) atom is surrounded by four cations with equivalent Bi(4)–A(1) distances of 3.247 (8) Å (A = Ca), 3.415 (3) Å (A = Sr) and 3.590 (1) Å (A = Ba). The terminal Bi(1) atoms are surrounded by a total of eight cations with distances of 3.221 (7)–3.384 (1) Å (A = Ca), 3.407 (3)–3.565 (1) Å (A = Sr), and 3.567 (1)–3.751 (1) Å (A = Ba).

The isolated Bi atoms in this structure form loosely associated pairs within a spiral coincident with the *c* axis. The Bi···Bi distances (4.15 Å (and 4.59 Å) (Ca), 4.33 Å (and 4.78 Å) (Sr), and 4.52 Å (and 4.94 Å) (Ba)) are considerably longer than any bonding interactions observed in any Bi compounds[14-16,24,25] and are not considered to be bonded to each other or to any other Bi atoms. Each Bi atom in the spiral has seven cations with distances of 3.201 (7)–3.349 (8) Å (Ca), 3.342 (3)–3.492 (3) Å (Sr), and 3.496 (2)–3.660 (2) Å (Ba).

Magnetic and Electrical Properties. Table IV summarizes the important magnetic parameters and a description of the magnetic properties follows: $Ca_{14}MnBi_{11}$ and $Sr_{14}MnBi_{11}$ were found to be ferromagnets with $T_C \approx$ 55 and 33 K, respectively, while $Ba_{14}MnBi_{11}$ is an antiferromagnet with $T_N \approx 15$ K.[17c] Fitting the high-temperature paramagnetic susceptibility to a Curie–Weiss law yielded Weiss constants, θ, of 50 (1), 38 (1), and 17 (1) K, for A = Ca, Sr, and Ba, respectively. These θ's are close to the observed transition temperatures, and are all positive, indicating ferromagnetic ordering. For $Ba_{14}MnBi_{11}$, θ is positive even though the compound orders antiferromagnetically. Within a simple mean-field two-sublattice model of an antiferromagnet, this can be understood[29] as describing a situation where the ferromagnetic exchange coupling between magnetic ions within a sublattice is considerably stronger than the antiferromagnetic coupling between ions on different sublattices. The effective magnetic moment per formula unit μ_{eff}, deduced from the Curie constant, ranges from 4.8 to 5.0 μ_B, suggesting that there are four unpaired electrons localized about each Mn ion, and therefore supports the assignment of +3 for the Mn valence. The hysteresis loop measurements show spontaneous moments, μ_s, of about 2.5 μ_B and 2.7 μ_B for A = Ca and Sr, respectively, and a saturation moment of about 2.9 μ_B for A = Ba (the Ba compound has a transition to a high-moment state at a temperature-dependent magnetic field $H < 20$ kOe). These "ordered moments" are smaller than the 4 μ_B that one would have expected from the Curie constants. The difference may be attributed to the polarization of the conduction electrons. We are currently making specific heat measurements to examine this possibility. Because of the large distances between the manganese atoms (10–11 Å) and the absence of any covalent bonds between them, the magnetic coupling has been attributed to a Ruderman–Kittel–Kasuya–Yosida (RKKY) interaction between the localized moments via conduction electrons.[30]

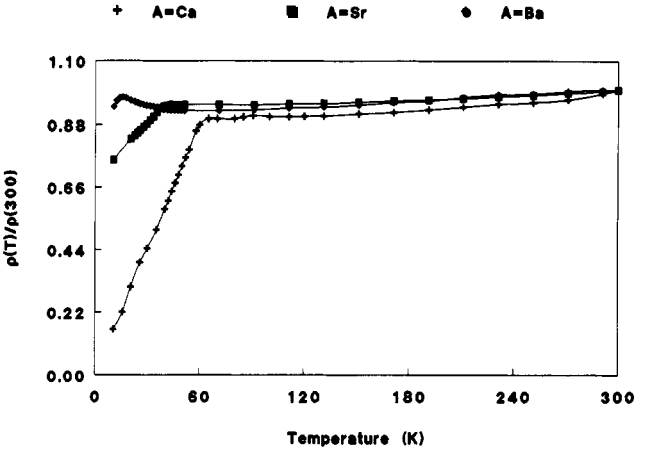

Figure 3. Plot of normalized resistivity ($\rho/\rho 300$) versus temperature for (Ca, Sr, Ba)$_{14}MnBi_{11}$ for 11 K < T < 300 K.

Standard four-probe dc resistivity measurements have been made on a polycrystalline piece of $Ca_{14}MnBi_{11}$ and on pressed pellets of $Sr_{14}MnBi_{11}$ and $Ba_{14}MnBi_{11}$. All of the samples are extremely air and water sensitive, and crystals obtained so far have been too small for a four-lead resistivity measurement. Figure 3 is a plot of the relative resistivities versus temperature of all three samples. Table IV provides the room-temperature resistivity value. The resistivity of $Ba_{14}MnBi_{11}$ and $Sr_{11}MnBi_{11}$ are higher (~1 (1) × 10^{-2} Ω cm) than $Ca_{14}MnBi_{11}$ (~8 (2) × 10^{-4} Ω cm), but the temperature dependences suggest that all three are metallic (i.e., the resistivity decreases as the temperature is reduced). Although 10^{-2} Ω cm is a rather high resistance for a metal, it is expected that the value for single crystals would be lower than the values measured on pressed pellets, suggesting, along with the temperature dependence of the data, metallic conduction. Many of the heavy pnictide (Sb, Bi) main-group metal Zintl compunds have been described as having a metallic luster.[3,4] As the heavier analogues are prepared, one expects the transition from semiconducting to semimetallic or metallic conductivity. The data for all samples have a sharp decrease in their resistivities below their magnetic ordering temperatures. This behavior is common for ferromagnets composed of both local magnetic ions and conduction electrons and is well understood in terms of the theory of de Gennes and Friedel.[31] The sharp drop in the resistivity at the ordering temperature results from a decrease in spin-disorder scattering of conduction electrons because of the ordering of the magnetic lattice. The resistivity of $Ba_{14}MnBi_{11}$ shows behavior similar to the other compounds down to around 60 K. At 60 K its resistivity begins to increase and peaks at the antiferromagnetic ordering temperature for $Ba_{14}MnBi_{11}$ (T_N = 15 K). A rise in resistivity as an ordering temperature is approached from high temperature can be seen in many antiferromagnetic

(27) Arduengo, A. J. III; Dixon, D. A. Electron-Rich Bonding at Low-Coordination Main Group Element Centers. In *Heteroatom Chemistry*; Block, E. Ed.; VCH Publishers Inc.: New York, 1990; p 47.
(28) Gallup, R. F.; Fong, C. Y.; Kauzlarich, S. M. *Inorg. Chem.*, in press.
(29) Kittel, C. *Introduction to Solid State Physics*; Wiley: New York, 1986; p 458.
(30) Kittel, C. *Solid State Phys.* **1968**, *22*, 1.
(31) de Gennes, P.-G.; Friedel, J. *J. Phys. Chem. Solids* **1958**, *4*, 71.

compounds as well as in some doped semiconductor ferromagnets (as predicted in ref 31). The rise in these cases is due to the fact that magnetic fluctuations above the ordering temperature have a length scale on the order of the length scale of the conduction electrons (inverse of the Fermi wavevector, k_F), and this matching of length scales makes for more efficient scattering by the fluctuating magnetic ions. The change from ferromagnetism in $Ca_{14}MnBi_{11}$ and $Sr_{14}MnBi_{11}$ to antiferromagnetism in $Ba_{14}MnBi_{11}$ may be attributed to a decrease in k_F. The RKKY interaction oscillates in sign as k_FR is changed (where R is the distance between magnetic ions), so a decrease in k_F can cause a change in sign resulting in an antiferromagnetic ground state. The near-neighbor interaction may become small and antiferromagnetic, while the next-near-neighbor magnetic interaction at larger k_FR stays ferromagnetic and large. This is consistent with antiferromagnetic order appearing in a compound which has a positive θ.

The rise in resistivity as the temperature is lowered in $Ba_{14}MnBi_{11}$ is also reminiscent of heavy Fermion compounds where the excess scattering is due to the formation of a Kondo-like Fermi liquid state as the temperature is decreased. In this compound we have an ordered magnetic state at low T which is quite unlike the heavy Fermion compounds, but at the present time, we cannot rule out the influence of this type of conduction electron local moment interaction. Specific heat measurements on these compounds are currently underway to confirm our interpretation of the magnetic and transport properties.

Acknowledgment. We thank M. M. Olmstead for assistance with the structure determinations. The diffraction and computing equipment used in the structure determinations was purchased under National Science Foundation Grant CHE-8802721. We thank R. N. Shelton for use of the magnetometer and P. Klavins for assistance in resistivity measurements. Financial support from the University of California, Davis and the National Science Foundation, Division of Materials Research (DMR-8913831 and DMR-8913855) is gratefully acknowledged.

Registry No. $Ca_{14}Bi_{11}Mn$, 122744-53-0; $Bi_{11}MnSr_{14}$, 136939-46-3.

Supplementary Material Available: Additional diffraction and refinement data and anisotropic displacement parameters for $A_{14}MnBi_{11}$ (3 pages); tables of observed and calculated structure factors (16 pages). Ordering information is given on any current masthead page.

Binary Thin Films from Molecular Precursors. Role of Precursor Structure in the Formation of Amorphous and Crystalline FeB

Chang-Soo Jun and Thomas P. Fehlner*

Department of Chemistry and Biochemistry, University of Notre Dame, Notre Dame, Indiana 46556

Gary J. Long*

Department of Chemistry, University of Missouri—Rolla, Rolla, Missouri 65401

Received October 17, 1991. Revised Manuscript Received December 18, 1991

The ferraboranes $B_2H_6Fe_2(CO)_6$ and $[B_2H_4Fe_2(CO)_6]_2$ have been investigated as volatile precursors for the deposition of thin iron boride films with composition FeB. The thermal decomposition of $B_2H_6Fe_2(CO)_6$ on glass or aluminum substrates at 175–250 °C at pressures between 10^{-5} and 10^{-4} Torr results in the deposition of uniform, amorphous alloy films of average composition $Fe_{56}B_{44}$ contaminated with 2–4% carbon and oxygen impurities. Individual film thicknesses ranged from 1000 to 6000 Å. Mössbauer effect spectra of these films, when compared with those from films prepared from $HFe_3(CO)_9BH_4$, show that a random packing model does not apply and that local structure exists in these films. Crystallization of these films at 600 °C followed by X-ray diffraction and Mössbauer spectroscopic examination reveals the formation of two phases, namely, Fe_2B and FeB. Although the structures of these two phases are the same as those produced by conventional high-temperature routes, the latter phase exhibits significantly different Mössbauer behavior. Utilization of $[B_2H_4Fe_2(CO)_6]_2$ as a precursor yields films of similar composition. Crystallization leads again to Fe_2B and FeB and no significant differences in the films formed from the two different precursors were observed.

Introduction

In previous studies[1-3] we have demonstrated that $HFe_4(CO)_{12}BH_2$ and $HFe_3(CO)_9BH_4$ can serve as precursors for thin alloy films with Fe/B ratios tracking those in the molecular precursor clusters even if the actual Fe/B ratios are not precisely those of the precursor cores. In spite of complications caused by carbon and oxygen impurities derived in part from the cleavage of CO, many of the properties of these well-formed films, e.g., magnetic properties, approach those of $Fe_{80-x}B_{20+x}$ ribbons formed via rapid quenching techniques.[4] Rapid quenching techniques are restricted to materials with compositions near the eutectic composition, whereas the vapor deposition of main-group transition-element clusters has, in

(1) Fehlner, T. P.; Amini, M. M.; Zeller, M. V.; Stickle, W. F.; Pringle, O. A.; Long, G. J.; Fehlner, F. P. *Mater. Res. Soc. Symp. Proc.* **1989**, *131*, 413.

(2) Amini, M. M.; Fehlner, T. P.; Long, G. J.; Politowski, M. *Chem. Mater.* **1990**, *2*, 432.

(3) Thimmappa, B. H. S.; Fehlner, T. P.; Long, G. J.; Pringle, O. A. *Chem. Mater.* **1991**, *3*, 1148.

(4) Hasegawa, R. *Glassy Metals: Magnetic, Chemical, and Structural Properties*; CRC Press: Boca Raton, FL, 1983.

0897-4756/92/2804-0440$03.00/0